Cholesterol provides nonsacrificial protection of membrane lipids from chemical damage at air–water interface

Xinxing Zhang[a,b], Kevin M. Barraza[a,b], and J. L. Beauchamp[a,b,1]

[a]Noyes Laboratory of Chemical Physics, California Institute of Technology, Pasadena, CA 91125; and [b]The Beckman Institute, California Institute of Technology, Pasadena, CA 91125

Contributed by J. L. Beauchamp, February 6, 2018 (sent for review December 21, 2017; reviewed by Barbara J. Finlayson-Pitts and Richard N. Zare)

The role of cholesterol in bilayer and monolayer lipid membranes has been of great interest. On the biophysical front, cholesterol significantly increases the order of the lipid packing, lowers the membrane permeability, and maintains membrane fluidity by forming liquid-ordered–phase lipid rafts. However, direct observation of any influence on membrane chemistry related to these cholesterol-induced physical properties has been absent. Here we report that the addition of 30 mol % cholesterol to 1,2-dipalmitoyl-sn-glycero-3-phosphocholine (DPPC) or 1-palmitoyl-2-oleoyl-sn-glycero-3-phospho-(1′-rac-glycerol) (POPG) monolayers at the air–water interface greatly reduces the oxidation and ester linkage cleavage chemistries initiated by potent chemicals such as OH radicals and HCl vapor, respectively. These results shed light on the indispensable chemoprotective function of cholesterol in lipid membranes. Another significant finding is that OH oxidation of unsaturated lipids generates Criegee intermediate, which is an important radical involved in many atmospheric processes.

cholesterol | phospholipid | OH radical | chemoprotection | air–water interface

Cholesterol (chol) universally comprises up to 30 mol % of the lipids in eukaryotic plasma membranes (1). This large amount of cholesterol modulates a plethora of biophysical properties of lipid membranes. For both bilayer and monolayer membranes, experimental and theoretical efforts have provided evidence that cholesterol has unique abilities to increase the order of lipid packing (1–4), lower the permeability (5, 6), and maintain the fluidity and diffusion rate (1, 2, 4) at the same time. Lateral phase studies of cholesterol/phospholipid complexes show that the formation of a liquid-ordered phase (l_o) is responsible for the seemingly contradictory coexistence of tight packing and high fluidity in both monolayer and bilayer membranes (4, 7). The small, dynamic, tightly bundled cholesterol–lipid assemblies, known as lipid rafts in the l_o phase, are considered to be the microscopic mechanism for cholesterol's unique functions in bilayers and monolayers (8–10). To date, the indispensable roles of cholesterol in lipid membranes are mainly discussed in the context of physical properties, and studies targeting the biochemical functions of cholesterol in membranes are scarce. Does cholesterol play a chemical role that could ultimately affect health? Only a few studies have attempted to answer this question. It has been hypothesized that cholesterol might function as a sacrificial antioxidant since oxidized cholesterols (oxysterols) are often detected in blood (11). It has also been suggested that cholesterol can lower the damage of phospholipid layers caused by ionizing radiation-initiated oxidation, inferred by indirect means such as the measurement of the fluorescence lifetime of other additives (12, 13). The oxidation products were not identified in these studies.

Given that investigations of the biochemical as opposed to the biophysical role of cholesterol are long overdue, here we report the direct observation of cholesterol's function in reducing the chemical damage of the saturated lipid 1,2-dipalmitoyl-sn-glycero-3-phosphocholine (DPPC) and the unsaturated lipid 1-palmitoyl-2-oleoyl-sn-glycero-3-phospho-(1′-rac-glycerol) (POPG) monolayers resulting from exposure to oxidants and strong acids at the air–water interface. The role played by cholesterol in restructuring membranes in a manner that provides a chemoprotective function is summarized in Fig. 1. Interfacial monolayers of phospholipids are ubiquitous in nature, present as the coating of natural waters (14), comprising half of bilayer cell membranes, and 80 mol % of the exposed surface of pulmonary alveoli that is directly in contact with air, in which DPPC takes up to 50 mol % of all of the pulmonary phospholipids (15). Hence, lipid monolayers are often the frontier that engages destructive chemical processes. The chemical reactions in the current study are initiated by singularly potent hydroxyl radicals (OH) and hydrochloric acid (HCl) vapor, two representative chemicals that are able to chemically attack phospholipids in a manner that is potentially harmful to human health. OH is an oxidant that exists both in the atmosphere and in vivo (16–18). Its lifetimes in these two environments are ∼1 s (16) and 1 ns (18), respectively. Once inhaled or generated in vivo, it can rapidly attack virtually all molecular species. Present both in the atmosphere and in vivo, HCl is chosen as a representative strong acid, which can degrade membrane phospholipids through acid-catalyzed hydrolysis reactions (19).

Detailed experimental methods are provided in *Materials and Methods*. Briefly, monolayers of pure DPPC, pure POPG, 70 mol % DPPC/30 mol % chol, or 70 mol % POPG/30 mol % chol form at the ambient air–water interface of a 2-mm diameter water

Significance

Comprising 30 mol % of the lipids in cell membranes, cholesterol plays vital biophysical roles in monolayer and bilayer membranes. It increases the lipid-packing density and maintains high membrane fluidity. Most studies of cholesterol in membranes focus on its effects on membrane structure and physical properties, with only minimum concern for possible biochemical consequences that might accompany these changes. In this study, field-induced droplet ionization mass spectrometry is employed to directly measure the chemical degradation of monolayer phospholipids caused by potent reagents OH and HCl at the air–water interface. When added to the lipid layer, cholesterol serves a nonsacrificial chemoprotective function, inhibiting the substantial degradation of both 1,2-dipalmitoyl-sn-glycero-3-phosphocholine and 1-palmitoyl-2-oleoyl-sn-glycero-3-phospho-(1′-rac-glycerol) that occurs in the absence of cholesterol.

Author contributions: X.Z. and J.L.B. designed research; X.Z. and K.M.B. performed research; X.Z. performed calculations; X.Z. and J.L.B. analyzed data; and X.Z. and J.L.B. wrote the paper.

Reviewers: B.J.F.-P., University of California, Irvine; and R.N.Z., Stanford University.

The authors declare no conflict of interest.

[1]To whom correspondence should be addressed. Email: jlbchamp@caltech.edu.

Published online March 5, 2018.

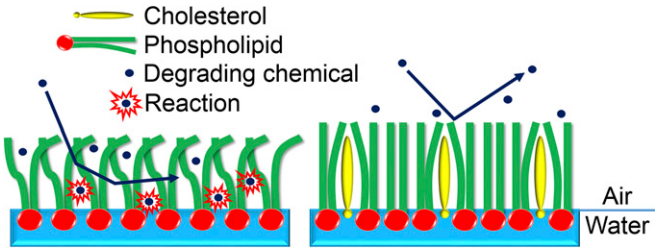

Fig. 1. Cartoon illustrating cholesterol's unique ability to increase the order of lipid packing and lower the permeability and subsequent reaction of degrading chemicals in lipid layers at the air–water interface.

droplet that is suspended on the end of a stainless steel capillary (Fig. 2). This molar ratio is chosen to reproduce the typical amount of cholesterol present in cell membranes. The OH radicals (1×10^9 molecule·cm^{-3}) are generated by a dielectric barrier discharge source (20), and the HCl vapor is from the evaporation of a Petri dish of 36.5% HCl solution placed underneath the droplet. The HCl vapor pressure is 114 mm Hg (21), corresponding to 3×10^{18} molecule·cm^{-3}. This number is significantly higher than the geographically highly variable ambient HCl concentration, which has been measured to be around 1 ppb (2.5×10^{10} molecule·cm^{-3}) in southern California (22). After being exposed to OH or HCl for a period of time, the compositions of the monolayers are determined using the interfacially sensitive field-induced droplet ionization mass spectrometry (FIDI-MS) methodology (Fig. 2) developed in our laboratory (23, 24). The zwitterionic DPPC is detected as a sodiated or protonated cation, POPG is detected as an anion (absent the Na^+ counterion), and cholesterol is protonated and sampled as a dehydrated cation.

Results

Fig. 3*A* presents the time-resolved oxidation of pure DPPC monolayer for 0-, 30-, 60-, and 90-s exposure to OH radicals, respectively. The *m/z* 757 peak is the sodiated DPPC parent cation, and the peaks with higher *m/z* are the oxidation products. These products are initiated by the abstraction of hydrogen atoms from the palmitoyl tails of DPPC by OH radicals, followed by steps mediated in part by ambient O_2 and NO molecules, forming carbonyl and hydroxyl functional groups (*vide infra*). At 90 s, ~90% of the DPPC is oxidized with the addition of one or more oxygen atoms. The absence of low mass products indicates that very little if any cleavage of C–C bonds results from OH-mediated oxidation. The average number of oxygen atoms per DPPC molecule as a function of oxidation time is shown in Fig. 3*C* as black squares. The observed linear behavior suggests that the heterogeneous surface oxidation process can best be described by Langmuir–Hinshelwood kinetics (20, 25). If OH reacted immediately on contact with the C–H bonds (Eley–Rideal kinetics), then the data in Fig. 3*C* would likely exhibit an upward curvature owing to the introduction of weaker and more reactive C–H bonds, such as the α-C–H bonds adjacent to a carbonyl group, at the air–water interface. Instead we argue that OH is accommodated at the surface with high probability, diffuses through the hydrocarbon layer, and eventually reacts by hydrogen abstraction. The extent of oxidation is hence determined by the constant flux of OH at the surface and over the course of time there is no acceleration or deceleration of the rate of oxygen incorporation. This is depicted by the cartoon on the left-hand side of Fig. 1.

Fig. 3*B* presents the products from the 70 mol % DPPC/30 mol % chol mixture monolayer following 180 s of exposure to OH at a density identical to that used in Fig. 3*A*. Surprisingly, with cholesterol present, DPPC is virtually immune to oxidation by OH radicals even after a much longer exposure time than in the absence of cholesterol, 180 s (Fig. 3*C*, red circles). It is thus evident that cholesterol acts to suppress oxidation. An obvious question arises from this observation. Is cholesterol playing a sacrificial role and oxidized in preference to DPPC, analogous to the antioxidant role played by vitamin C (26), or is the restructured tightly packed l_o phase of the chol/DPPC mixture blocking access of OH to the lipid? Fig. 3*B* shows that cholesterol is in the protonated dehydrated form (*m/z* 369) as expected when detected by MS (27), and no oxidation products are observed even though the C–H bond-rich cholesterol is expected to be vulnerable to OH attack. In light of this, it can be concluded that cholesterol is not sacrificial, and instead it restructures the lipid layer in a manner that greatly reduces the uptake of OH radicals, thus inhibiting the oxidation of both itself and DPPC. This is illustrated by the right-hand side of Fig. 1, which depicts the effect of cholesterol on lipid structure and packing.

According to Fig. 3*C*, it takes about 25 s for OH to oxidize DPPC with approximately one oxygen atom per lipid molecule. Since the OH concentration used in our study is three orders of magnitude higher than the ambient concentration, it would take 7 h to cause the same extent of oxidation by ambient OH radicals. When 30 mol % cholesterol is present, by a rough estimation using the data in Fig. 3*C*, the same extent of oxidative damage to pulmonary DPPC by inhaling ambient OH will be extended to more than 600 h!

Fig. 4*A* shows the OH oxidation of POPG for 0, 30, 60, and 90 s. The *m/z* 747 peak is the POPG parent anion. In complete contrast to the oxidation chemistry of the saturated palmitoyl groups of DPPC, the oxidation products of POPG appear at lower *m/z* as a result of introducing the unsaturated oleyl group. The oxidation chemistry of POPG is dominated by the highly reactive double bond of the oleoyl chain. The *m/z* 637 product is a result of the double bond cleaved into an aldehyde group, and the *m/z* 671 species is from the oxidation of the double bond into a hydroxyhydroperoxide (HHP) product via a Criegee intermediate (CI) (*vide infra*). Remarkably, CI is an important atmospheric radical resulting from the reaction of ozone with olefins (28), and a major contributor to OH radicals in the troposphere (29). Our results provide evidence that OH oxidation of unsaturated hydrocarbons can in turn generate CI. Fig. 4*D* presents the percent conversion to products versus oxidation time (black squares). The observed linear behavior indicates that the reaction is fast and limited by the OH flux at the air–water interface, again consistent with Langmuir–Hinshelwood kinetics (20, 25). Once more, cholesterol effects a remarkable suppression of oxidation and only a small fraction of the 70% POPG/30% chol mixture is oxidized after 180-s exposure time (Fig. 4 *B* and *D*, red circles). As with DPPC, cholesterol is not killed (Fig. 4*C*). From these results, it can be concluded that the presence of

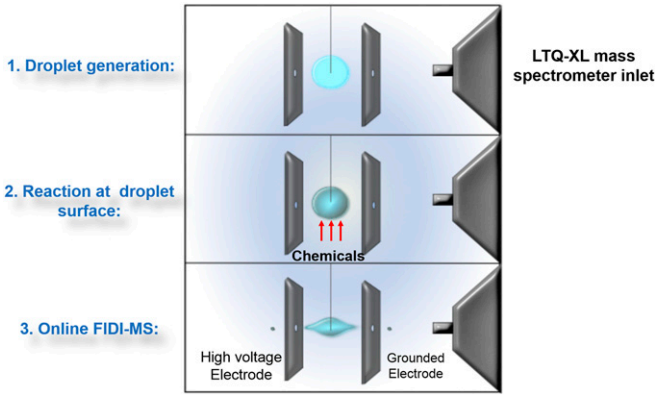

Fig. 2. Schematic drawing of the FIDI-MS setup and operation.

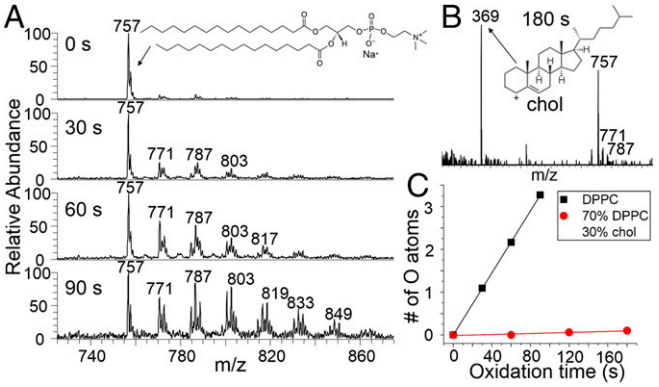

Fig. 3. Results from the OH oxidation of DPPC and cholesterol containing monolayers at the air–water interface. (*A*) Time-resolved cation-mode FIDI-MS spectra including the reactant and products from the pure DPPC monolayer. At 90 s, ~90% of the nascent lipid layer is oxidized by addition of one or more oxygen atoms, mainly in the form of multiple carbonyl and hydroxyl groups. (*B*) Cation-mode FIDI-MS spectrum including the reactant and products from the 70 mol % DPPC/30 mol % chol monolayer after 180 s of oxidation time. There is no evidence that cholesterol is oxidized and the extent of lipid oxidation is greatly reduced compared with that in *A*. (*C*) The average number of incorporated oxygen atoms per DPPC molecule as a function of time from the pure DPPC (black squares) and 70 mol % DPPC/30 mol % chol (red circles) monolayers.

30 mol % cholesterol significantly lowers the permeability of OH into monolayers comprising both saturated and unsaturated phospholipids at the air–water interface.

It is of interest to compare the different behavior of the saturated and unsaturated lipids observed in Figs. 3 and 4, respectively. The average number of oxygen incorporated into surface DPPC molecules increases linearly with time. This does not happen to a significant extent with POPG, indicating that the OH diffusing through the lipid layer reacts much more rapidly with the remaining unsaturated oleyl groups than it does with the already oxidized lipids. This is consistent with the gas-phase studies of the reactions of OH radicals with hydrocarbons, where it is observed that olefins are 10–100× more reactive than their saturated counterparts (30).

In Fig. 5 *A* and *C*, the time dependence of the acid-catalyzed hydrolysis of the ester bonds of a pure DPPC monolayer film resulting from exposure to HCl vapor is exhibited. The products involving loss of one of the palmitic acid (*m/z* 497) tails gradually increase in intensity with increasing exposure time, a direct evidence of acid-catalyzed hydrolysis. The addition of 30 mol % cholesterol to the lipid layer mitigates the hydrolysis process (Fig. 5*B*). After 180 s of exposure time, only 9% of DPPC is hydrolyzed (Fig. 5*C*, red circles). In the case of POPG (Fig. 6*A*), there are two possible hydrolysis products, the loss of oleic acid (*m/z* 483) and the loss of palmitic acid (*m/z* 509), observed in approximately equal amounts. Once again, the addition of cholesterol significantly reduces the hydrolysis of POPG caused by the HCl vapor (Fig. 6 *B* and *C*). As with OH radicals, it can be inferred that permeability of HCl is greatly reduced in the combined chol/lipid interfacial layer. This is an example of directly observed acid-catalyzed ester cleavage chemistry of membrane lipids at the air–water interface, demonstrating the efficacy of the FIDI methodology for studies of complex interfacial chemistry.

Discussion

Fig. 7 presents proposed mechanisms for the OH oxidations of POPG and DPPC. The OH oxidation of DPPC occurs at the two hydrophobic saturated alkyl chains that present at the air–water interface. Since the two palmitoyl tails are rich in reactive C–H bonds, they are all potential sites of reaction. In Fig. 7*A*, DPPC is simplified as $R_1CH_2R_2$. The reaction starts with step (1), a H atom abstraction by an OH radical, resulting in an alkyl radical. Afterward, the alkyl radical generated in step (1) can add an O_2 molecule to form a peroxy radical in step (2) since the concentration of ambient O_2 is many orders of magnitude higher than OH. Step (3) is the well-known mechanistic step that involves NO (31, 32). The ambient NO concentration in the Los Angeles area is typically $\sim 1 \times 10^{11}$ molecule·cm^{-3} (33), significantly higher than the OH concentration ($\sim 1 \times 10^{9}$ molecule·cm^{-3}) in the current study. NO will abstract an oxygen atom from the peroxy group to yield an alkoxy radical and NO_2. From this alkoxy radical, two different reactions can occur. It can either react with an O_2 molecule to form a carbonyl [step (4)] and a HO_2 leaving group, or abstract a H atom from ambient HO_2 to form a hydroxyl group [step (5)]. The ambient HO_2 concentration is typically $\sim 2 \times 10^{9}$ molecule·cm^{-3} (34). Both step (4) and step (5) are well-documented pathways in the reactions of OH with saturated hydrocarbons (30, 35). The formation of a carbonyl group adds 14 Da to the molecular weight, and the formation of a hydroxyl group adds 16 Da. The initial introduction of hydroxyl and carbonyl groups into saturated hydrocarbons creates sites where weakened C–H bonds are more likely to react further with OH by hydrogen abstraction and subsequently with O_2, NO, and HO_2 in accordance with Fig. 7*A*, resulting in more combinations of carbonyl (+14 Da) and hydroxyl groups (+16 Da) to the parent DPPC ion, this being accountable for the *m/z* 771 (DPPC + carbonyl), 773 (DPPC + hydroxyl), 785 (DPPC + 2 carbonyl), 787 (DPPC + carbonyl + hydroxyl), 789 (DPPC + 2 hydroxyl), 801 (DPPC + 2 carbonyl + hydroxyl), 803 (DPPC + carbonyl + 2 hydroxyl), 815 (DPPC + 3 carbonyl + hydroxyl), and 817 (DPPC + 2 carbonyl + 2 hydroxyl) product peaks in Fig. 3*A*. The continuing sequence of reactions ultimately leads to highly oxidized products, such as those observed in Fig. 3*A* after oxidation for 90 s, at which time ~90% of the surface exposed DPPC is oxidized with the addition of one or more oxygen-containing functional groups. Similar oxidation patterns of saturated hydrocarbons by OH radicals are observed for the 18-carbon chain of stearic acid at the air–water interface (20).

Fig. 7*B* depicts the reaction mechanisms proposed for the OH oxidation of POPG. Unlike DPPC, bond cleavage products are

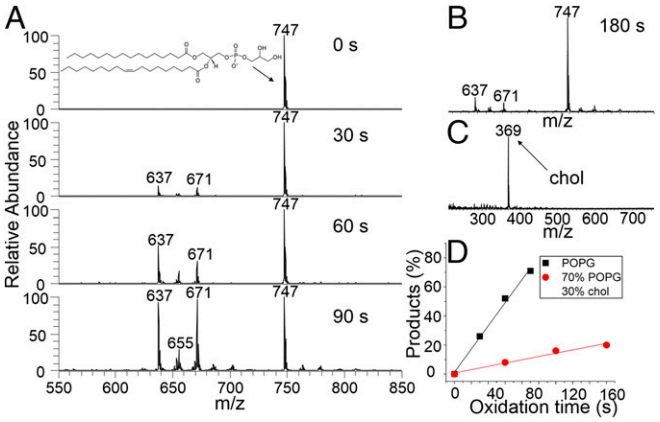

Fig. 4. Results from the OH oxidation of POPG and cholesterol-containing monolayers at the air–water interface. (*A*) Time-resolved anion-mode FIDI-MS spectra including the reactant and products from the pure POPG monolayer. (*B*) Anion-mode FIDI-MS spectrum including the reactant and products from the 70 mol % POPG/30 mol % chol monolayer after 180 s of oxidation time. The extent of lipid oxidation is greatly reduced compared with that in *A*. (*C*) Cation-mode FIDI-MS spectrum showing chol from the 70 mol % DPPC/30 mol % chol monolayer after 180 s of oxidation time. There is no evidence that cholesterol is oxidized. (*D*) Products percentage as a function of time from the pure POPG (black squares) and 70 mol % POPG/30 mol % chol (red circles) monolayers.

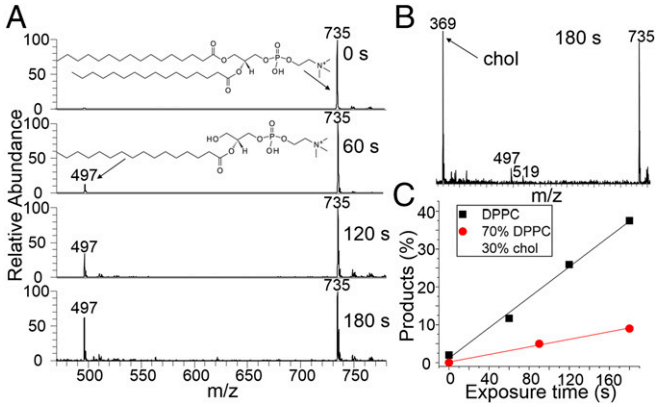

Fig. 5. Results from the HCl vapor degradation of DPPC and cholesterol-containing monolayers at the air–water interface. (*A*) Time-resolved cation-mode FIDI-MS spectra including the reactant and products from the pure DPPC monolayer. (*B*) Cation-mode FIDI-MS spectrum including the reactant and products from the 70 mol % DPPC/30 mol % chol monolayer after 180 s of exposure time. The extent of lipid degradation is greatly reduced compared with that in *A*. (*C*) Products percentage as a function of time from the pure DPPC (black squares) and 70 mol % DPPC/30 mol % chol (red circles) monolayers.

preferred in this case. Step (1) is the heterogeneous uptake of an OH radical from the gas phase by the double bond at either the ω − 9 or the ω − 10 carbon, resulting in two different β-hydroxyalkyl radicals (35). It is reasonable to postulate that OH attaches to the ω − 9 and ω − 10 carbon atoms with similar probabilities since they are both near the middle of the monolayer, having similar accessibilities to the gas-phase OH radicals. After OH addition, step (2) involves uptake of an O_2 molecule to form two different β-hydroxyperoxy radicals, one of which can undergo β-cleavage to an α-hydroxyalkyl radical [step (3)], and the latter can further react with O_2 to form a HO_2 leaving group and an aldehyde molecule [*m/z* 637, step (4)]. The aldehyde reacts with H_2O to form the hemiacetal product [*m/z* 655, step (5)]. The second β-hydroxyperoxy radical formed in step (2) can also undergo thermal dissociation into a CI and a hydroxyalkyl radical [step (6)]. This CI product, written in its favored zwitterionic form, can react with the CI scavenger, H_2O, to form the *m/z* 671 HHP product [step (7)]. This HHP product is a symbolic evidence of the CI reaction pathway (36) and eventually becomes an abundant product. To further confirm the CI pathway, two other CI scavengers (37), methanol and ethanol, were also utilized by forming droplets comprising water/methanol or water/ethanol (1/1) solutions. Since methanol and ethanol can be viewed as the OH group in water replaced by a methoxy or ethoxy, it is anticipated that the products are methoxyhydroperoxide (MHP, *m/z* 685) and ethoxyhydroperoxide (EHP, *m/z* 699), 14 and 28 Da, respectively, more than the HHP product. The products are accordingly observed with the respective mixed solvent droplets (Fig. 8). Since water is present in the droplets of all of the three systems along with ambient atmospheric water and helium flow seeded water vapor from the DBD source, HHP is observed in all three experiments. There are also several other hemiacetal product peaks in Fig. 8 resulting from the reaction between the aldehyde (*m/z* 637) and water, methanol, or ethanol. Fig. 7*B* depicts the proposed reaction mechanism, including steps involving methanol and ethanol. The aldehyde generated in step (4) can react with H_2O, MeOH, or EtOH to form the corresponding hemiacetal products [step (5)]. The CI generated in step (6) reacts with H_2O, MeOH, or EtOH to form the HHP, MHP, or EHP products in step (7).

To explore the energetics associated with formation of the CI, potential energy surface calculations using C_2H_4 as a model system are presented in Fig. 9. All of the structures are optimized at the ωB97X-D/6–311++G(3df, 3pd) (38) level of theory with zero-point energy corrected using the Gaussian09 package (39). The ωB97X-D functional was chosen because of its good performance in describing long-distance interactions such as hydrogen bonding. The addition of OH and O_2 to C_2H_4 lowers the energy from 0 to −1.27 and −2.63 eV, respectively. Mediated by O_2, the β-hydroxyperoxy radical can dissociate into a HO_2 radical, a formaldehyde molecule, and a CI, which is 0.55 eV lower in energy than the reactants. The reaction between CI and H_2O to yield HHP further lowers the energy to −2.35 eV. Hence, the CI pathway is overall thermodynamically favored for the C_2H_4 model system, providing more confidence in the proposed mechanism in Fig. 7*B*. The structure of CI is reoptimized at the coupled-cluster level of theory using singlet, doublet, and perturbative triplet excitations [CCSD(t)] (40) with the same basis set, and the atomic charge is calculated with the natural population analysis methods (41). The calculations on the properties of CI, including the bond lengths, angles, atomic charges and its further reaction with water closely reproduced published results (42). One concern relating to the calculated reaction pathway is the bond cleavage step that forms the CI, which involves an energy increase of 2.11 eV. This seems a somewhat high barrier to overcome, since the energy gain from the first two steps will be quickly dissipated in the condensed-phase environment. We speculate that there might be other molecules such as water that can mediate the reaction and significantly lower this energy barrier. Such a phenomenon was observed between CI (from the gas phase) and water at the air–water interface, where the reaction rate leading to HHP is increased by 2–3 orders magnitude by the participation of other water molecules (43).

It is of particular interest that the OH oxidation products of POPG are very different from those of the OH oxidation of oleic acid (20), where the double bond is oxidized by adding carbonyl groups instead of being cleaved, even though the reactive oleyl functional groups are the same in both cases. This difference might be due to constraints imposed by the much higher packing density of POPG compared with that of oleic acid at the air–water interface (44, 45). The OH oxidation products of DPPC and POPG in this study are also different from the OH oxidation products of DPPC and 1-palmitoyl-2-oleoyl-sn-glycero-3-phosphocholine (POPC) studied at the surface of micrometer-size NaCl particles and characterized by diffuse reflectance infrared spectroscopy and

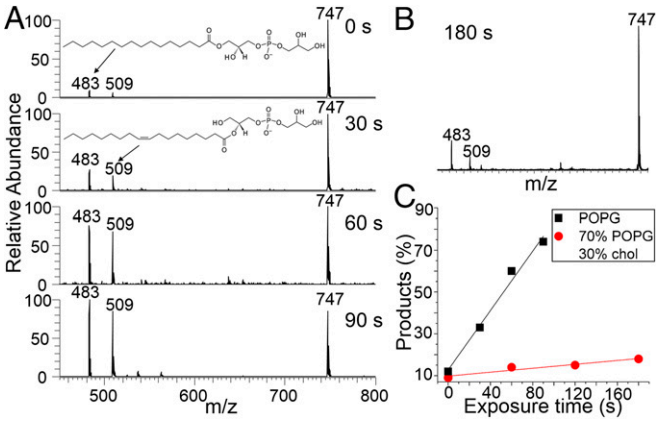

Fig. 6. Results from the HCl vapor degradation of POPG and cholesterol-containing monolayers at the air–water interface. (*A*) Time-resolved anion-mode FIDI-MS spectra including the reactant and products from the pure POPG monolayer. (*B*) Anion-mode FIDI-MS spectrum including the reactant and products from the 70 mol % POPG/30 mol % chol monolayer after 180 s of exposure time. The extent of lipid degradation is greatly reduced compared with that in *A*. (*C*) Products percentage as a function of time from the pure POPG (black squares) and 70 mol % POPG/30 mol % chol (red circles) monolayers.

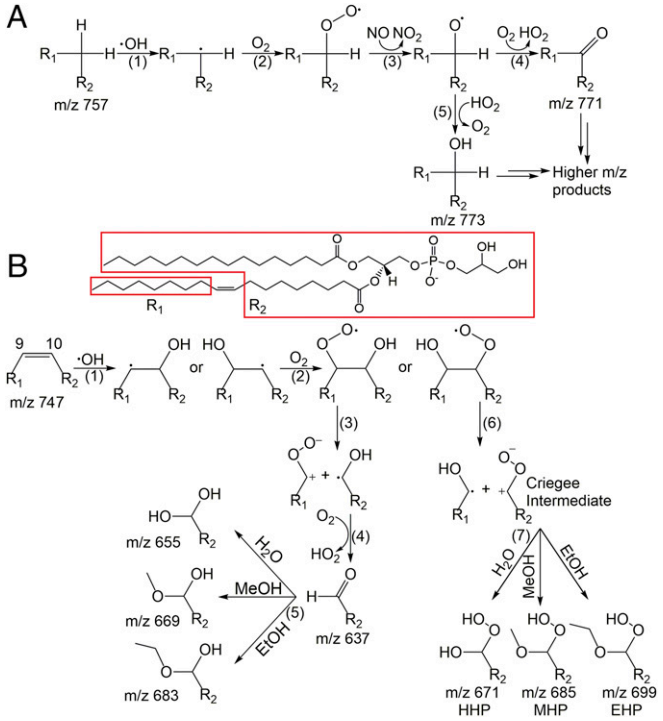

Fig. 7. Proposed mechanisms of OH oxidation of (*A*) DPPC and (*B*) POPG.

MALDI-TOF-MS (46). POPC and POPG have the same fatty acid tails. This difference once again might be a result of the lipid-packing difference at the air–water interface and the air–NaCl interface.

For the reactions initiated by HCl, molecular dynamics simulations show that the fatty acid ester linkages are submerged in the aqueous portion of the air–water interface (47). We propose that HCl dissociates to lower the interfacial pH and effect acid-catalyzed hydrolysis of the ester linkages. Note that the two ester linkage sites are not chemically equivalent and the oleyl ester bond is slightly more submerged at the interface. This might lead to more effective solvation of the transition state for hydrolysis and contribute to the slightly higher abundance of the corresponding product observed in Fig. 6 *A* and *B*.

Based on the above-presented results and mechanisms, and the observation that cholesterol itself is not oxidized in any of these experiments, it can be concluded that cholesterol protects membrane lipids from chemical damage at the air–water interface by increasing the packing density of the lipids and lowering the permeability of the lipid layer to potent degrading chemicals such as OH and HCl.

Conclusion

To conclude, saturated and unsaturated membrane lipids DPPC and POPG alone at the air–water interface can be greatly damaged by OH radicals and HCl. The OH oxidation of saturated lipids results in adding multiple oxygen-containing functional groups, such as hydroxyl or carbonyl, to the alkyl chains. In contrast, OH oxidation of unsaturated lipids prefers to cleave the double bond of the fatty acid chain. Remarkably, our results provide evidence that OH oxidation of lipids incorporating unsaturated fatty acids can generate CI, an important species generated by the ozonolysis of olefins in the atmosphere (28). Mechanisms for these reactions have been proposed in Fig. 7. The damage caused by HCl to membrane lipids at the air–water interface is accounted for by acid-catalyzed hydrolysis reactions, resulting in loss of the fatty acid chains. The addition of 30 mol % cholesterol to the interfacial phospholipids restructures lipid layers in a manner that significantly lowers their permeability by OH and HCl in lipid layers at the air–water interface, substantially precluding the chemical damage initiated by these species (Fig. 1). Cholesterol itself is not sacrificial in these reactions. Nature has endowed cholesterol-containing membranes with physical properties that afford protection from degradation by potent chemical agents.

Materials and Methods

DPPC and POPG were purchased from Avanti Polar Lipids and used without further purification. Cholesterol (≥99%) was purchased from Sigma-Aldrich and used without further purification. All solvents (water and methanol) are HPLC grade and purchased from EMD Chemicals Inc. Solutions of 2 mM of DPPC, POPG, and cholesterol are firstly obtained by dissolving the chemicals in methanol, and then diluted by water to make solutions of 100 μM pure DPPC, 100 μM pure POPG, 70 μM DPPC/30 μM cholesterol mixture, and 70 μM POPG/30 μM cholesterol mixture for experimental use.

Fig. 2 presents the schematic drawing of the FIDI-MS setup. Briefly, a hanging droplet of ~2 mm o.d. (~4 μL in volume) is suspended on the end of a stainless steel capillary between two parallel plate electrodes separated by 6.3 mm. Droplets are formed from liquid fed through the capillary using a motorized syringe pump. The parallel plates are mounted on a translation stage to allow alignment of an aperture in the electrically grounded plate with the atmospheric pressure inlet of an LTQ-XL mass spectrometer (Thermo-Fisher). The capillary is mounted on a separate translation stage to place the droplet exactly midway between the two plates and to align with the inlet of the LTQ-XL. Mass spectrometric sampling of the hanging droplet is accomplished by applying a pulsed high-voltage (typically 3–5 kV, 100-ms duration, polarity subject to change according to the ions that are sampled) to the back parallel plate and to the capillary at half the magnitude applied to the back plate to maintain field homogeneity between the front and back plate. When a sufficiently high voltage is applied, bipolar ejection of highly charged progeny droplets less than 1 μm in diameter from the opposite ends of the suspended droplet is generated. Charged droplets of a specific polarity enter the transfer capillary of the mass spectrometer, resulting in the detection of gas-phase ions. In this study, we apply positive voltage on the back plate to detect the protonated dehydrated cholesterol, sodiated or protonated DPPC and related cations, and negative voltage to detect desodiated POPG and related anions. When each droplet is initially formed, we allow 60 s for the molecules to diffuse to the air–water interface before exposing the droplet to hydroxyl radicals or HCl vapor for a variable reaction time. After the reactions, we trigger the high voltage to sample both reactants and products. Sampling occurs on a millisecond time scale. Each experiment starts with a fresh drop.

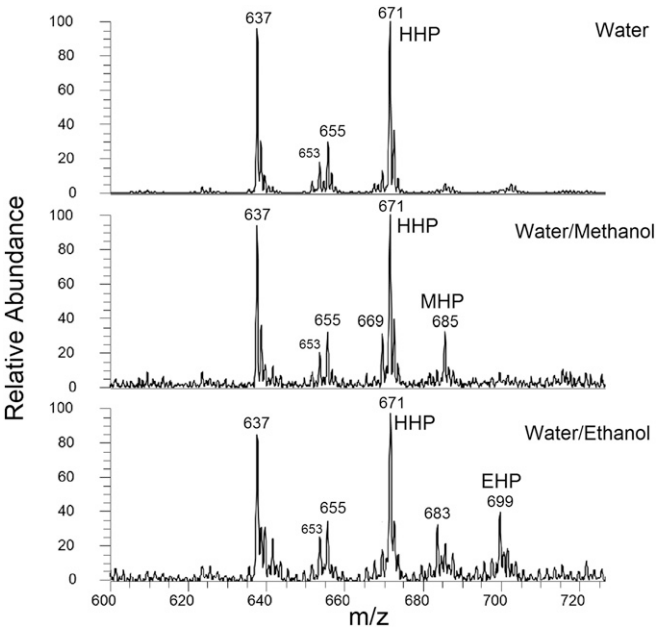

Fig. 8. Mass spectra showing the products of the OH oxidation of the POPG anion in droplets comprising water, 1/1 water/methanol, and 1/1 water/ethanol solutions. The expected products, HHP, MHP, and EHP, are observed from the reactions between the CI and water, methanol, and ethanol, respectively.

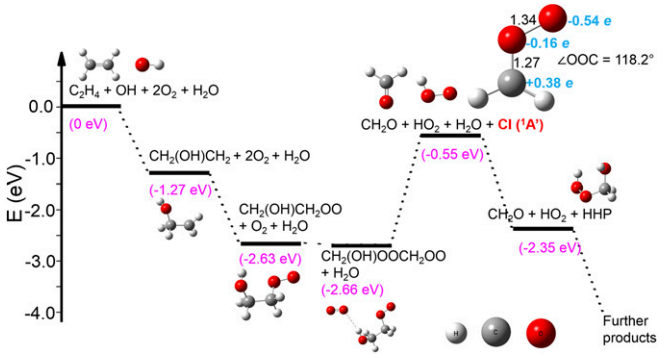

Fig. 9. Relative energies (electron volts) for the formation and depletion of CI using ethylene as a model system. The calculated properties of CI, including the bond lengths (angstroms), ∠OOC bond angle (degrees), and atomic charge obtained from natural population analysis (e) are also presented.

Hydroxyl radicals are generated using a dielectric barrier discharge source (DBDS) composed of a borosilicate tube (1/4-in o.d., 3/16-in i.d.) which acts as the dielectric material. A tungsten filament inner electrode is sealed within the tube, and a conductive silver epoxy coating (McMaster-Carr) acts as an outer electrode. A glass bubbler provides water-saturated helium through the DBDS, with a flow of 1,000 mL/min monitored by a type πMFC Digital Mass Flow Controller (model PFC-50; MKS Instruments). A high-voltage ac power supply (Trek PM04015) biased the inner electrode during experiments at 12 kV (peak to peak) and 1,000 Hz, while the outer electrode remained grounded. Between the power supply and the tungsten filament, there is a 1-MΩ resistor used as a current limiter. A low-temperature plasma (dielectric barrier discharge) is generated inside the tube, producing hydroxyl radicals in the gas flow. Compared with the tropospheric OH radical concentration that was measured to be 1–3 × 10^6 molecule·cm^{-3} (16), the DBDS can generate ∼1 × 10^9 molecule·cm^{-3} OH radicals (20) based on the time required to oxidize a monolayer of surfactant with an average of one oxygen per surfactant molecule. The high intensity of OH radicals significantly accelerates the oxidation process compared with ambient conditions.

The reactions initiated by HCl vapor are performed by placing a Petri dish of fresh 36.5% HCl solution underneath the droplet. The dish is big enough to encompass the whole area of the FIDI setup, so that each droplet can be exposed to a steady and homogeneous HCl vapor environment.

ACKNOWLEDGMENTS. This work was supported by the Beckman Institute at Caltech and by NSF Grant CHE-1508825.

1. Mouritsen OG, Zuckermann MJ (2004) What's so special about cholesterol? *Lipids* 39: 1101–1113.
2. Simons K, Ikonen E (2000) How cells handle cholesterol. *Science* 290:1721–1726.
3. MacDermaid CM, et al. (2015) Molecular dynamics simulations of cholesterol-rich membranes using a coarse-grained force field for cyclic alkanes. *J Chem Phys* 143: 243144.
4. Yuan C, Johnston LJ (2008) Phase evolution in cholesterol/DPPC monolayers: Atomic force microscopy and near field scanning optical microscopy studies. *J Microsc* 130: 11883–11885.
5. Szabo G (1974) Dual mechanism for the action of cholesterol on membrane permeability. *Nature* 252:47–49.
6. Jurak M (2013) Thermodynamic aspects of cholesterol effect on properties of phospholipid monolayers: Langmuir and Langmuir-Blodgett monolayer study. *J Phys Chem B* 117:3496–3502.
7. de Meyer F, Smit B (2009) Effect of cholesterol on the structure of a phospholipid bilayer. *Proc Natl Acad Sci USA* 106:3654–3658.
8. Simons K, Ikonen E (1997) Functional rafts in cell membranes. *Nature* 387:569–572.
9. Lingwood D, Simons K (2010) Lipid rafts as a membrane-organizing principle. *Science* 327:46–50.
10. Ando J, et al. (2015) Sphingomyelin distribution in lipid rafts of artificial monolayer membranes visualized by Raman microscopy. *Proc Natl Acad Sci USA* 112:4558–4563.
11. Smith LL (1991) Another cholesterol hypothesis: Cholesterol as antioxidant. *Free Radic Biol Med* 11:47–61.
12. Parasassi T, et al. (1995) Cholesterol protects the phospholipid bilayer from oxidative damage. *Free Radic Biol Med* 19:511–516.
13. Lasch J, Schönfelder U, Walke M, Zellmer S, Beckert D (1997) Oxidative damage of human skin lipids. Dependence of lipid peroxidation on sterol concentration. *Biochim Biophys Acta* 1349:171–181.
14. Estillore AD, Trueblood JV, Grassian VH (2016) Atmospheric chemistry of bioaerosols: Heterogeneous and multiphase reactions with atmospheric oxidants and other trace gases. *Chem Sci (Camb)* 7:6604–6616.
15. Nkadi PO, Merritt TA, Pillers D-AM (2009) An overview of pulmonary surfactant in the neonate: Genetics, metabolism, and the role of surfactant in health and disease. *Mol Genet Metab* 97:95–101.
16. Isaksen ISA, Dalsøren SB (2011) Atmospheric science. Getting a better estimate of an atmospheric radical. *Science* 331:38–39.
17. Karam LR, Bergtold DS, Simic MG (1991) Biomarkers of OH radical damage in vivo. *Free Radic Res Commun* 12-13:11–16.
18. Sies H (1993) Strategies of antioxidant defense. *Eur J Biochem* 215:213–219.
19. De Koning AJ, McMullan KB (1965) Hydrolysis of phospholipids with hydrochloric acid. *Biochim Biophys Acta* 106:519–526.
20. Zhang X, Barraza KM, Upton KT, Beauchamp JL (2017) Time resolved study of hydroxyl radical oxidation of oleic acid at the air-water interface. *Chem Phys Lett* 683:76–82.
21. Fritz JJ, Fuget CR (1956) Vapor pressure of aqueous hydrogen chloride solutions, 0° to 50° C. *Ind Eng Chem Chem Eng Data Series* 1:10–12.
22. Eldering A, et al. (1991) Hydrochloric acid: A regional perspective on concentrations and formation in the atmosphere of southern California. *Atmos Environ Part A* 25:2091–2102.
23. Grimm RL, Beauchamp JL (2003) Field-induced droplet ionization mass spectrometry. *J Phys Chem B* 107:14161–14163.
24. Grimm RL, Beauchamp JL (2005) Dynamics of field-induced droplet ionization: Time-resolved studies of distortion, jetting, and progeny formation from charged and neutral methanol droplets exposed to strong electric fields. *J Phys Chem B* 109: 8244–8250.
25. Ammann M, Pöschl U, Rudich Y (2003) Effects of reversible adsorption and Langmuir–Hinshelwood surface reactions on gas uptake by atmospheric particles. *Phys Chem Chem Phys* 5:351–356.
26. Padayatty SJ, et al. (2003) Vitamin C as an antioxidant: Evaluation of its role in disease prevention. *J Am Coll Nutr* 22:18–35.
27. Johnson DW, ten Brink HJ, Jakobs C (2001) A rapid screening procedure for cholesterol and dehydrocholesterol by electrospray ionization tandem mass spectrometry. *J Lipid Res* 42:1699–1705.
28. Criegee R (1975) Mechanism of ozonolysis. *Angew Chem Int Ed Engl* 14:745–752.
29. Liu F, Beames JM, Petit AS, McCoy AB, Lester MI (2014) Infrared-driven unimolecular reaction of CH_3CHOO Criegee intermediates to OH radical products. *Science* 345:1596–1598.
30. Calvert JG, et al. (2000) *The Mechanism of Atmospheric Oxidation of the Alkenes* (Oxford Univ Press, New York).
31. King MD, Thompson KC (2003) Rate constants for the reaction of NO and HO_2 with peroxy radicals formed from the reaction of OH, Cl or NO_3 with alkenes, dienes and α, β-unsaturated carbonyls. *Atmos Environ* 37:4517–4527.
32. Calvert J, Derwent RG, Orlando JJ, Tyndall GS, Wallington TJ (2008) *Mechanisms of Atmospheric Oxidation of the Alkanes* (Oxford Univ Press, New York).
33. Westerdahl D, Fruin S, Sax T, Fine PM, Sioutas C (2005) Mobile platform measurements of ultrafine particles and associated pollutant concentrations on freeways and residential streets in Los Angeles. *Atmos Environ* 39:3597–3610.
34. Martinez M, et al. (2003) OH and HO_2 concentrations, sources, and loss rates during the southern oxidants study in Nashville, Tennessee, summer 1999. *J Geophys Res* 108:4617–4633.
35. Finlayson-Pitts BJ, Pitts JN, Jr (1999) *Chemistry of the Upper and Lower Atmosphere* (Academic, San Diego).
36. Chao W, Hsieh J-T, Chang C-H, Lin JJ-M (2015) Atmospheric chemistry. Direct kinetic measurement of the reaction of the simplest Criegee intermediate with water vapor. *Science* 347:751–754.
37. Tobias HJ, Ziemann PJ (2001) Kinetics of the gas-phase reactions of alcohols, aldehydes, carboxylic acids, and water with the C13 stabilized Criegee intermediate formed from ozonolysis of 1-tetradecene. *J Phys Chem A* 105:6129–6135.
38. Chai JD, Head-Gordon M (2008) Long-range corrected hybrid density functionals with damped atom-atom dispersion corrections. *Phys Chem Chem Phys* 10:6615–6620.
39. Risch MJ, et al. (2009) *Gaussian 09, Revision A.1* (Gaussian, Inc., Wallingford, CT).
40. Raghavachari R, Trucks GW, Pople JA, Head-Gordon M (1989) A fifth-order perturbation comparison of electron correlation theories. *Chem Phys Lett* 157:479–483.
41. Reed AE, Curtiss LA, Weinhold F (1988) Intermolecular interactions from a natural bond orbital, donor-acceptor viewpoint. *Chem Rev* 88:899–926.
42. Long B, Bao JL, Truhlar DG (2016) Atmospheric chemistry of Criegee intermediates: Unimolecular reactions and reactions with water. *J Am Chem Soc* 138:14409–14422.
43. Zhu C, et al. (2016) New mechanistic pathways for Criegee–water chemistry at the air/water interface. *J Am Chem Soc* 138:11164–11169.
44. Han S (2013) Molecular dynamics simulation of oleic acid/oleate bilayers: An atomistic model for a ufasome membrane. *Chem Phys Lipids* 175-176:79–83.
45. Rose D, Rendell J, Lee D, Nag K, Booth V (2008) Molecular dynamics simulations of lung surfactant lipid monolayers. *Biophys Chem* 138:67–77.
46. Dilbeck CW, Finlayson-Pitts BJ (2013) Hydroxyl radical oxidation of phospholipid-coated NaCl particles. *Phys Chem Chem Phys* 15:9833–9844.
47. Ko JY, Choi SM, Rhee YM, Beauchamp JL, Kim HI (2012) Studying interfacial reactions of cholesterol sulfate in an unsaturated phosphatidylglycerol layer with ozone using field induced droplet ionization mass spectrometry. *J Am Soc Mass Spectrom* 23: 141–152.